INITIAL GEOMETRIC IMPERFECTIONS: A ROBUST, CLOSED-SECTION COLD-FORMED BOX PROFILE APPLICATION SUBJECT TO LOCAL BUCKLING

N.Brambatti Junior, M.Walber[*] and A.D.de Meira Junior
University of Passo Fundo, BRASIL
E-mail: mwalber@upf.br

Initial geometric imperfections are important for simulating local buckling in numerical models. References are found in the technical literature regarding open-section cold formed profiles. This work presents new procedures applied to a robust and closed-section cold formed profile subject to local buckling, and the use of procedures described in the technical literature already successfully used for open section profiles. The difference of this work in relation to the research already carried out is in the type of profile studied, in the mode of failure of the same and in the form of determination of the initial imperfections. The object of study of this work is a closed-section cold formed box profile with a short length when compared with its cross section and with local buckling failure mode. The strategies used in the present work to consider the initial geometric imperfections were to perform the linear stability analysis using the finite element method to obtain the local buckling mode that represents the deformed box profile geometry, to apply a multiplication factor in the displacements, replace the new geometry node coordinates for all profile nodes to induce the local buckling deformation mode, with model validation through experimental testing and the Effective Width Method (MLE) (ABNT NBR 14762 [1]). Finally, using the results of the collapse load of the experimental trial as a basis, it was possible to compare the results obtained by MLE and MEF. Thus, the presentation of this work used a methodology that describes the local buckling behavior and verified the precepts of the existing norms on the subject, combining theoretical and experimental methods, as they bring a better understanding of the structural problem in question.

Keywords: Bucket elevator, box profile, local buckling, finite element method, experimental test, initial geometric imperfections.

1. Introduction

The main contribution of this work is the presentation of new procedures applied to a robust and closed-section cold formed box profile, and the use of procedures described in the technical literature already successfully used for open section profiles.

The use of geometric imperfections in the numerical model of the object of study is an important step of the analysis, as they will induce the failure due to the local buckling effect. There is no consensus on how to treat geometric imperfections in numerical models; however, it is known that the shape, magnitude and mode of application of geometric imperfections constitute a sensitive factor in the simulation to obtain the mode of collapse.

Currently the most commonly used ways to introduce geometric imperfections in the numerical model are by surveying the actual dimensions of the imperfections found in the profiles under analysis or by using the deformed geometry of the buckling mode [2-6] found by linear stability analysis using the method of finite elements or considering recommendations of codes and standards [7-16]. After obtaining the deformed geometry of the buckling modes of the box profile submitted to a centered compression load, which originates from the chosen buckling mode, these new geometries are replaced for all profile nodes.

---

[*] To whom correspondence should be addressed

The difference of this work in relation to the research already carried out is in the type of profile studied, in the mode of failure of the same and in the form of determination of the initial imperfections. The object of study of this work is a box profile with a short length when compared with its cross section and with local buckling failure mode. The strategies used in the present work to consider the initial geometric imperfections were to perform the linear stability analysis using the finite element method to obtain the local buckling mode that represents the deformed closed-section cold formed box profile geometry, to apply a multiplication factor in the displacements of the nodes, replace the new geometry node coordinates for all profile nodes in order to induce the deformation mode, with model validation through experimental testing and the Effective Width Method (EWM). Through the MEF analysis, confirmed by experimental centered compression test, it is observed that the lateral of the box profile evolves its configuration of deflections until in the instant immediately before the local buckling collapse it presents a two-curve shape.

Another contribution of this work is the evaluation of other values for the magnitude of box profile imperfections (multiplication factors with values of *0*, *20*, *1*, *2*, *3*, *4* and *5*), besides those proposed by Schafer and Pekoz [12] that for type *1* initial geometric imperfections (standard ABNT NBR 14762 [1], type AA elements, which are evaluated in the box profile due to local buckling mode) use a relationship between the maximum size of the imperfection and the thickness of the plate cold formed profile with a value of *0.14*.

The trough profile instability analysis method proposed in this work is a suitable alternative to conventional eigenvalue based methods. Unlike open profiles, the profile formed by the box profile is closed and robust, which gives it a great resistance after buckling. Thus, the box profile when subjected to compressive stresses presents a great resistance after buckling and collapse due to the effect of local buckling. In a box profile cross-section formed by "flat panels" (flat side of the box) fixed to "curved panels" (the folds), the action of a compression load produces a redistribution of stresses such that their strength it is mainly established in the sheet folds that make up the box profile. This feature of the profile geometry makes the eigenvalue method difficult to predict the instability load because the actual collapse load of the profile is larger than the load calculated by the method.

The initial geometric imperfections, as applied in this work, do not sensitize the result of the collapse load, since the main support of the compression load in the box profile is in the folds due to stress redistribution. The side of the box profile has little contribution to the strength of the profile, where the initial geometric imperfections were attributed. However, the attributions of the initial geometric imperfections are very important in the compression load analysis as they serve as a guide for deflections in order to reproduce the actual failure mode observed in the local buckling trial.

The choice for the analysis of a box profile used in grain elevators in grain storage silos has an economic and social justification. In the maintenance of the silos, to remove obstructions to the movement of the grains, work in height and in confined spaces is required. Workers are exposed to the risk of explosion, fire, noise, fall, among other risks, which generate a high number of accidents. Structural engineering can help to avoid unsafe conditions for workers by developing safe system designs of adequate dimensions to avoid them.

Methodologies that better describe the local buckling behavior and verify the precepts of the existing norms on the subject, combining theoretical and experimental methods, contribute as they bring a better understanding of the problem in question.

The case study presented to illustrate the proposed methodology is to investigate the structural behavior of the box profile used in the bucket elevator as well as to define its load and collapse form. For this purpose, it will be presented as a methodology to approach the problem first to present the methodology of determination of the initial geometric imperfections, then to define the axial load of collapse through the standard ABNT NBR 14762 [1] on sizing of steel structures made of cold formed profiles, then to experimentally test the box profile to validate the considerations made in the numerical model simulation and finally evaluate the structural behavior of the box profile numerical model through the finite element method and define the axial load of collapse, considering the methodology for determining and using imperfections initial geometric.

The trunking, shown in Fig.1a, is joined by flanges, which are fixed in the box profiles shown in Fig.1b. The box profile, object of study, is formed by two cold formed sections and linked by joining sheet metal clinching (SMC).
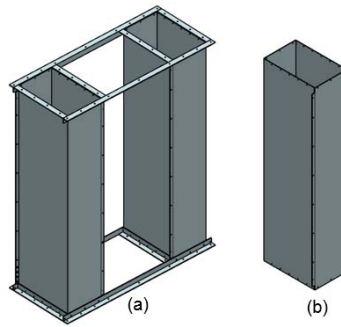
Fig.1: (a) Trunking; (b) Box profile.

2. Initials geometric imperfections and their considerations in numerical simulation

Differences in parallelism, perpendicularity, and slope are some characteristics that differentiate a well-modeled geometric surface, in error-free engineering software, from a real effective surface. These differences between the geometric and effective surface are called geometric imperfections.

In a slender profile or plate that forces on its central axes to compress them, they are said to be under centered compression. However, due to their geometric imperfections and possible eccentricities, they are actually under flexion-compression. Lateral displacements then occur in their constituent elements, resulting in additional stresses that in turn may compromise maximum compressive strength.

Young [17] suggested a sinusoidal function to roughly represent the initial global imperfection (δ) due to a compression load (N) in a length profile (L), represented in Figure 2. It is acceptable in many cases due to variation of the imperfections found in practice, Young's [17] approximation was used as the basis for the resistance curves in American and European standards. However, Young's proposal does not represent the imperfections located in a profile, and it is usually those imperfections that will cause the collapse due to the effect of local or distortion buckling.
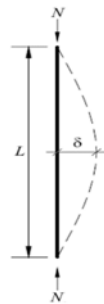

Fig.2. Global imperfection suggested by Young [17].

Currently the most commonly used ways to introduce geometric imperfections in the numerical model are manual or automatic. The manual form consists of making a survey of the real dimensions of the imperfections found in the profiles under analysis and using them to create the numerical model that will be analyzed. Lecce and Rasmussen [4] used this method in their work, making laboratory measurements by a laser to use the effective surfaces in the models under analysis.

The automatic form, used in this work, is based on the use of the deformed buckling mode geometry found by linear stability analysis. Stability analysis via finite element program provides the values of the critical forces and the corresponding buckling modes. Thus, the pure modes, isolated and non-combined modes, referring to local, distortion and global buckling modes are applicable. The mesh node coordinates of this new finite element model geometry are updated to simulate the stability analysis nonlinearly.

According to Chodraui [11] there is still no consensus on how to treat geometric imperfections in numerical models. However, it is known that the shape, magnitude and mode of application of geometric imperfections constitute a sensitive factor in the simulation to obtain the forces of collapse. Chodraui [11] conducts a theoretical and experimental analysis of open section profiles (stiffened U, U profiles and single and double angles) and cold formed. For the attribution of the initial geometric imperfections, he performed a numerical linear stability analysis of the profiles that provides as a result the value of the critical force and the deformed geometry of the profile. From the result of the deformed configuration for each of the isolated buckling modes (local, global and distortion when applicable), these new geometries were superimposed for all profile nodes. As a means of analyzing the sensitivity to the amplitude of these imperfections, the criterion adopted was the use of the magnitudes of the initial geometric imperfections through a probabilistic analysis of the work of Schafer and Pekoz [12].

Sousa [18] conducted a theoretical and experimental analysis of the stability of perforated columns of the open-section and cold-formed rack profile. In the same way as Chodraui [11] he performed the attributions of geometric imperfections through the linear stability analysis of the profile with the overlapping of the isolated buckling modes. However, the choice of buckling mode and magnitude of imperfection was made through the experimental measurements of the specimens submitted to compression tests.

Bonatto [16] in his master's dissertation, useed the same procedure as Chodraui [11] for the attribution of geometric imperfections in his numerical models, regarding the study of the structural behavior of cold formed angles. Triches [6] also used the overlapping of isolated buckling modes for the attribution of geometric imperfections, but as an amplification factor of the displacements of deformed geometry nodes reusds the thickness of the profiles.

2.1. Methodology for placing initial geometric imperfections in numerical simulation

The object of study of this work is a closed box profile a short length when compared with its cross section and with local buckling failure characteristic.
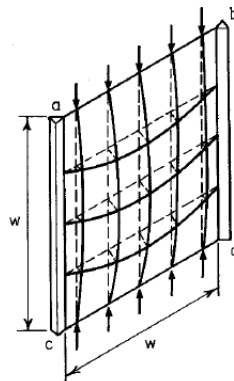

Fig.3. Plate subjected to compressive stresses under the action of post buckling resistance [19].

The profile formed by the box is closed and robust, which has a great resistance to buckling. Thus, the box profile when subjected to compressive stresses does not collapse under the critical buckling stress, but exhibits high post-buckling strength and yield collapse due to the effect of local buckling. Unlike open one-dimensional structural elements, rigid elements of a profile under compression stress will not collapse under critical buckling stress. There will be a redistribution in the stresses of the profile element, which means an extra load supported by it. This phenomenon is known as post buckling resistance.

Figure 3 represents the action of the post buckling resistance in a plate subjected to the action of compressive stresses. Now the buckling of the element begins and its horizontal bars will act as tie rods attached to the vertical supports at the edges of the plate to decrease deflection perpendicular to the surface of the plate.

Alves Filho [20] observed that for box-type cross sections, where there is a change in cross-section geometry due to it being formed by "flat panels" (flat side of the rail) fixed in "curved panels" (the folds), the action of a compression load causes a redistribution of stresses, such that its resistance is established mainly in the bends of the sheet that make up the profile of the box. This characteristic of the profile geometry makes the eigenvalue method difficult to predict the instability load because the actual collapse load of the profile is much larger than the calculated load. Therefore, one of the alternatives for the analysis of box type profile instability is the methodology of the present research.
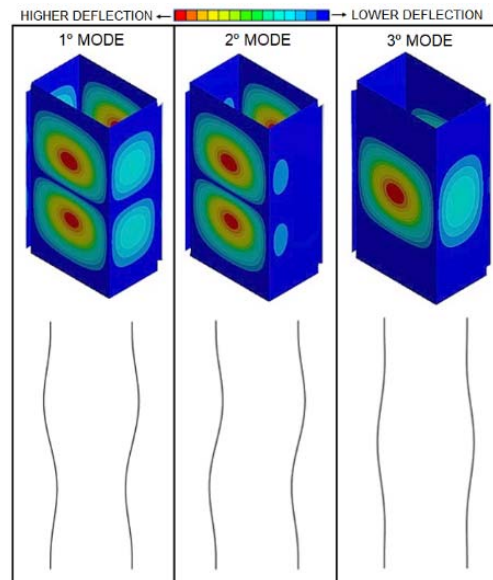

Fig.4. Deformed configuration of the first three buckling modes of the centered compression box profile.

Thus, the strategy used in the present work to consider the initial geometric imperfections was to perform the linear stability analysis via finite element program to obtain the local buckling mode that best represents the deformed box profile geometry and obtain the geometry deformed from the local buckling modes of the box profile, through the coordinates of the deformed mesh nodes, which originates from the chosen buckling mode. You can also use a multiplication factor to apply to node offsets, similar to the magnification scale that is used in plotting results. For the present work, the multiplication factor will be used to give the magnitude of the geometric imperfections in the box profile body, which will be analyzed to verify how sensitive this factor is to its collapse load.

Following the objectives of the work, geometric imperfections will be attributed only in the body of the box profile. Thus, the surface model was created in a Computer Aided Design (CAD) program without considering the box profile joint flanges and cold forming plate-joining points between the profiles.

In a local buckling, the side of the box profile evolves its deflection configuration until the moment immediately before the collapse it presents a two-curve shape with inverted curvature. To choose the buckling mode, which through its deformed geometry will represent and assign the geometric imperfections in the finite element numerical model, it will be necessary to understand the evolution of the lateral deflections of the box profile as the compression load is applied. As the compression load is applied, the side of the box profile forms a deflection curve in the external direction of its cross section, effect of which can be observed in Fig.4, first mode. However, when the box profile is very close to collapse, the side of the box profile forms two deflection curves, approximately half externally and half internally of its cross section.

Thus, the attributions of geometric imperfections in the numerical model for nonlinear analysis will be from the deformed configuration of the first elastic linear buckling mode.

The values (δ) of the initial geometric imperfections were taken as the apex of the deflection curve of the first buckling mode, as shown in Fig.5, which was used to assign them. The initial geometric imperfections were measured in the direction of load application, as it is estimated that they will have the greatest effect on the collapse load and box profile deflections.

In the work of Schafer and Pekoz [12], geometric imperfections were classified into two types. Type 1 are imperfections relative to type AA cold formed profile elements (their two edges linked to curved elements). Type 2 are imperfections relative to cold formed AL profile elements (a bounded edge on a curved element and a free edge). Because the box profile has only AA type elements and collapse due to the effect of local buckling mode, attention will paid to geometric imperfections of type 1.

Schafer and Pekoz [12] describe that for initial type 1 geometric imperfections, with a ratio of d/t (where d is the maximum imperfection size and t is the thickness of the cold formed profile plate) and with a value of *0,14* there is a *75 %* chance that the database of imperfections collected in the literature will exceed the values adopted for numerical analysis. This value will be used as a reference for the magnitude of the initial geometric imperfections, but other values will also be evaluated to try identifying the influence of the magnitude of the imperfections on the box profile, which is the object of study of this research.
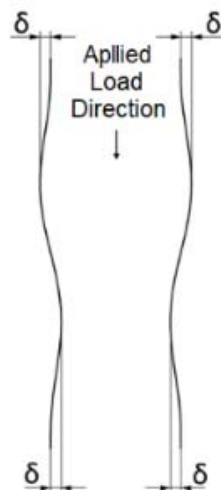
Fig.5. Position of values of initial geometric imperfections.

The initial geometric imperfections do not have the function of sensitizing the result of the collapse load. As previously described, the main support of the compression load in the box profile is in the folds due to stress redistribution. Thus, the side of the box profile has little contribution to the strength of the profile, the position where the initial geometric imperfections were attributed.

However, it is noteworthy that the attributions of the initial geometric imperfections are very important in the analysis under compression load. They also serve as a guide for deflections so that the box profile collapses in the form of two bends. For if there were no imperfections in the box profiles, it would simply lower its height and present a constant tension across its side, which is not the reality.

3. Structural analysis of box profile via effective width method (EWM)

The assessment was initiated by the effective width method (EWM), as described in the standard ABNT NBR 14762 [1]. Due to the experimental equipment available to the experimental test which present limited conditions on clearance and maximum compression load, an experimental model was created, which through the EWM mode it possible to assess the appropriate dimensions for the test.

3.1. Model with original dimensions versus experimental model

The box profile with the dimensions used in the trunking of a bucket elevator will be described as model with the original dimensions (MOD). It features rectangular cross section of *584mm×365mm*, *2000mm* height and *2,70mm* sheet thickness.

The box profile that will be used in the test is described as an experimental model (EM). It has the same cross section dimensions as the model with original dimensions, *1100mm* height and *1,55mm* sheet thickness.

Table 1 presents the mechanical properties of the material used in the box profile, where f_y is the yield stress, f_u is the ultimate tensile stress, E is the Young modulus, G is the shear modulus and ν is the Poisson ratio.

Table 1. Mechanical properties of the material.

$f_y\,(MPa)$	259,83
$f_u\,(MPa)$	307,90
$E\,(GPa)$	200
$G\,(GPa)$	77
ν	0,3

The properties f_y and f_u were extracted from the tension test, which origins will be described later. The properties *E, G* and ν were extracted from standard ABNT NBR 14762 [1].

Table 2. Geometric property of the sections.

	MOD	EM
$t\,(mm)$	2,70	1,55
$A\,(mm^2)$	5077	2926
$L\,(mm)$	2000	1100
$I_x\,(mm^4)$	252077200	146077520
$I_y\,(mm^4))$	123791944	71826280
$J\,(mm^4))$	254734768	147170784
$C_w\,(mm^6))$	$2{,}5452 \times 10^{11}$	$1{,}4705 \times 10^{11}$
$r_o\,(mm)$	272,1	272,89
$b_a\,(mm)$	354,2	
$b_b\,(mm)$	573,2	

Table 2 presents the geometric properties of the sections, where L is the height of the section, I_x is the moment of inertia about the x-axis and I_y in the y-axis, J is the torsion constant of the cross section, C_w is the torsional warping constant of the cross section, r_o is the polar radius of gyration of the cross section

about shear center, b_a and b_b are the widths of the elements of sections for analysis in the EWM. The coordinate system and the real cross section dimensions are shown in Fig.6.
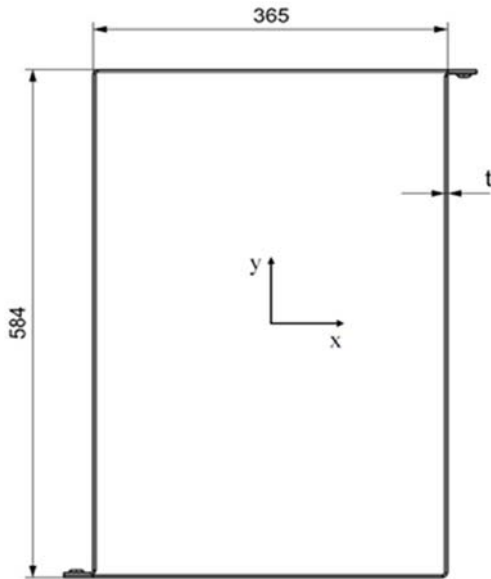

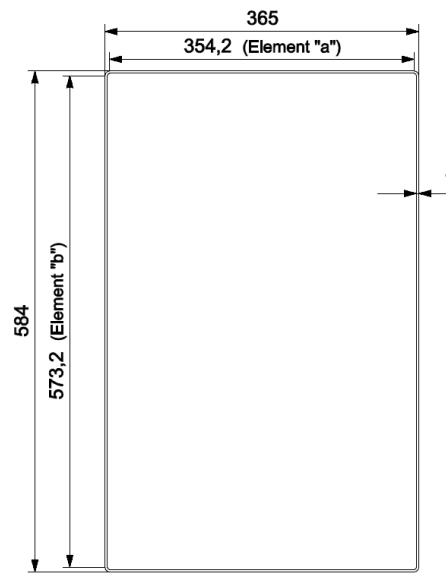| Fig.6 Dimensions of the real box profile cross section. | Fig.7. Dimensions of the simplified cross section of the box profile. |

3.2. Calculation procedure: standard ABNT NBR 14762 [1]

The EWM is one of the methods presented in the Brazilian standard calculation for design of cold-formed sections. As introduced by von Karman *et al*. [21], instead of considering non-uniform distribution of the stresses applied along the width of the sheet, it is considered that the whole load is being supported by a fictional width, called effective width, subjected to uniform compression stresses along the width. More details of this concept can be found in Yu [19].

According to Carvalho *et al*. [22], the standard assumes that the section is a combination of sheets, elements, thereby uses the EWM to consider the effect of buckling in each of these elements in isolation, obtaining a section with effective geometric properties.

The cross section of the box profile has been simplified as a rectangle with *90* -degree bends in its four edges, as shown in Fig.7.

The following is the procedure used for the calculation of the available axial compressive strength of cold-formed sections (standard ABNT NBR 14762 [1]).

Through Eqs (3.1), (3.2) and (3.3) the axial strength for flexural and torsional overall buckling are obtained:

$$N_{ex} = \frac{\pi^2 E I_x}{\left(K_x L\right)^2} ,$$
(3.1)

$$N_{ey} = \frac{\pi^2 E I_y}{\left(K_y L\right)^2} ,$$
(3.2)

$$N_{ez} = \frac{1}{r_o^2}\left(\frac{\pi^2 E C_w}{(K_z L)^2} + GJ\right).$$

(3.3)

In Eqs (3.1), (3.2) and (3.3) K is the effective length factor and the other properties were defined previously. At this point you can get the value of the effective slenderness factor related to the overall buckling (λ_o), given by (3.4).

$$\lambda_o = \left(\frac{A f_y}{N_e}\right)^{0,5}$$

(3.4)

where N_e is the smallest value of the three axial strength for the overall buckling. Then we obtain the value of the compression strength reduction factor (χ) through Eq.(3.5). The χ represents the iteration between the local and global buckling of a section subjected to compressive stresses

$$\lambda_o \leq 1,5 : \chi = 0,658^{\lambda_o^2},$$

$$\lambda_o > 1,5 : \chi = \frac{0,877}{\lambda_o^2}.$$

(3.5)

By Eq.(3.6) you can calculate the critical stress of the section.

$$\sigma = \chi \cdot f_y.$$

(3.6)

Then, Equation (3.7) defines the reduced slenderness factor of element (λ_p):

$$\lambda_p = \frac{b/t}{0,95\left(kE/\sigma\right)^2}.$$

(3.7)

In Eq.(3.7), b is the width of the element of the section and k is the plate-buckling coefficient of element. As the analysis is for centered load the element is under uniform compression stress, this way, standard ABNT NBR 14762 [1] defines that the value of k is 4. Equation (3.8) to obtain the effective width of the element.

$$\lambda_p \leq 0,673 : b_{ef} = b,$$

$$\lambda_p > 0,673 : b_{ef} = \frac{b}{\lambda_p}\left(1 - \frac{0,22}{\lambda_p}\right).$$

(3.8)

Therefore, to define the available axial compressive strength $(N_{c,Rd})$ of cold-formed section we use Eq.(3.9):

$$N_{c,Rd} = \chi \, A_{ef} f_y \tag{3.9}$$

where, A_{ef} cis the effective area of the cross section. The load factor indicated by the standard for the calculation of $N_{c,Rd}$ was disregarded considering that this value will be compared directly with the values of the experimental test.

3.3. Results and discussions: the effective width method

Conducting an analysis of λ_o and χ based on values of K, it can be foreseen what will be the form of collapse of the analyzed section can be foreseen.

Table 3 presents the recommended values of the effective length factor (K) related to the various end support conditions, obtained according to standard ABNT NBR 8800 [23].

Table 3. Recommended values of effective length factor.

End Support condition	K
Two ends with prevented rotation and translation	*0,65*
One end rotation and prevented translation and one end with free rotation and prevented translation	*0,8*
Two ends with free rotation and prevented translation	*1*
One end with prevented rotation and translation and one end with prevented rotation and free translation	*1,2*
One end with free rotation and prevented translation and one end with prevented rotation and free translation	*2*
One end with prevented rotation and translation and one end with free rotation and translation	*2,1*

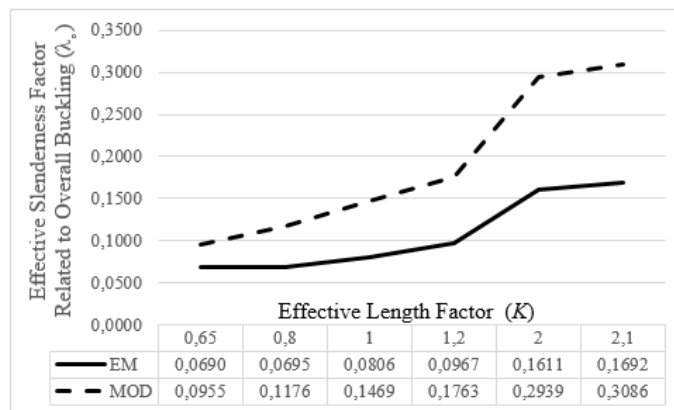|	0,65	0,8	1	1,2	2	2,1
EM	0,0690	0,0695	0,0806	0,0967	0,1611	0,1692
MOD	0,0955	0,1176	0,1469	0,1763	0,2939	0,3086

Fig.8. Index values λ_o in function of the values of the coefficient K.

Figure 8 shows the index values λ_o and Fig.9 shows the values of the factor χ, both in function of the values of the coefficient K, presented in Tab.3.
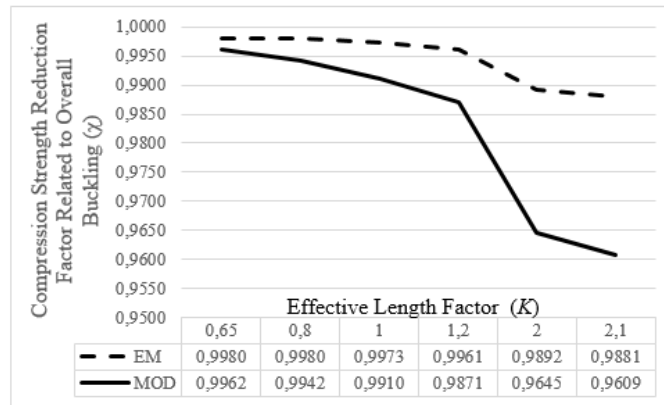
Fig.9. Factor values χ in function of the values of the coefficient *K*.

It is observed that the index λ_o has little variation because of the end support conditions and little influence on the proportional reduction factor χ, which in all situations remains of values close to one.

The reduction factor χ represents the iteration between the local and global buckling of a section subjected to compressive stresses and it is also used to calculate the critical stress (σ), which will rule the conditions of equilibrium between stability and instability of the section. Figure 10 shows the values of the available axial compressive strength $\left(N_{c,Rd}\right)$ due to the values of the coefficient K.
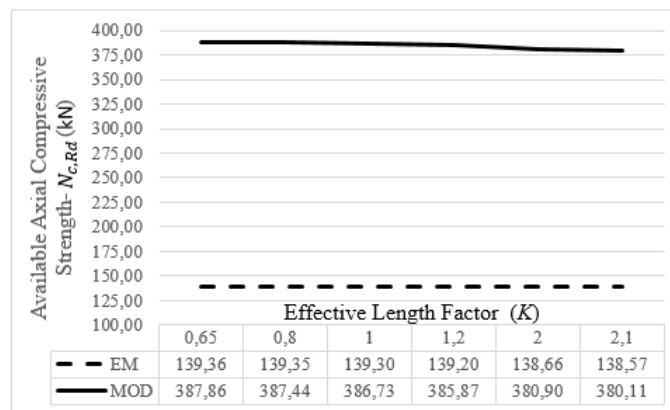

Fig. 10. Values of the available axial compressive strength in function of the values of the coefficient *K*.

The value of the coefficient *K* as *2.1* was used concerning the condition of support indicated in Tab.3. The same was chosen to represent the condition used in the experimental test. Through Fig.9 and Eq.(3.6), it is noted that the stress σ values are *98,8* % for the EM and *96,1* % for the MOD of the yield stress f_y .

Therefore, with the slenderness factor λ_o low values, and consequently, with the reduction factor χ with values close to 1, and also due to the little influence of strength $N_{c,Rd}$ in function of the end support conditions, shown in Fig.10, we can predict that the collapse of the sections are associated with close to yield stress values of the material. Next, the way of collapse will be predominantly influenced by the effect of local buckling. In sections with predominance of the global buckling effect, the strength $N_{c,Rd}$ would show a significant variation in function of the values of the coefficient *K*. The strength values $N_{c,Rd}$ that will be used as a basis for comparison with other methods are *138,57kN* for EM and *380,11kN* for MOD.

4. Experimental test of centered compression of the box profile

This section presents the procedures and results of the compression test with experimental centered box profile loading. The results of experimental tests will be used as a basis for comparison to other methods. The concentric compression test was conducted on four test samples shown in Fig.11.
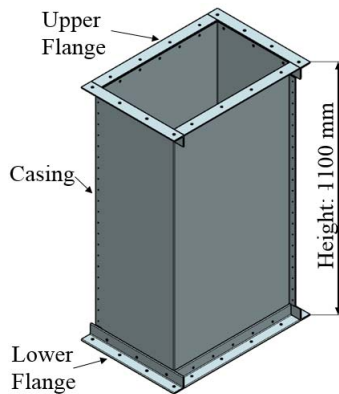

Fig.11. Experimental model (EM) of the box profile for testing of centered compression.

Fig.12. Gantry to be used in compression testing.

They all were subject to the same considerations and measurements. The material used in the box profile is low carbon hot rolled steel plate with zinc plated finish.

4.1. Equipment, devices and instrumentation

The gantry shown in Fig.12 was used as structure for fixing the load application equipment and other devices It has a vertical clearance of *1700mm* and free width *1220mm*. When the hydraulic cylinder and the base sections have been assembled on the gantry, their vertical clearance will be at *1250mm*, that is why the experimental model was built with a height of *1100mm*.

Hydraulic cylinder with manual override was used for application of compression load. It has a maximum stroke of *300mm* and maximum load capacity of *30000kgf*, therefore the experimental model was built with *1,55mm* plate thickness. According to EWM calculus, the collapse load of the experimental model of the box profile is *138,57kN*, getting below the maximum load capacity of the hydraulic cylinder.

A load cell LPX-50 TON MK brand with SOLOTEST brand signal reception system was used for the measurement of the compression load. It has a maximum record capacity of *50000kgf*. Figure 13b shows the general configuration of the assembly of equipment, devices and instrumentation for the experimental test. Figure 13a shows the instrumentation for sheet displacement measurement in the perpendicular direction to, where two LVDT (Linear Variable Differential Transformer) and a dial indicator gauge were used. Figure 13c shows instrumentation for the evaluation of the displacement box profile in the direction of the compression load application, where two dial indicators were used. Figure 13d shows the hydraulic cylinder for application of the compression load and load cell for its measuring.
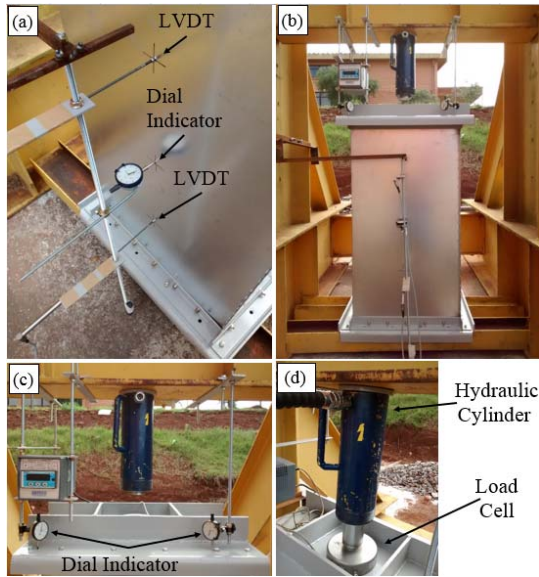
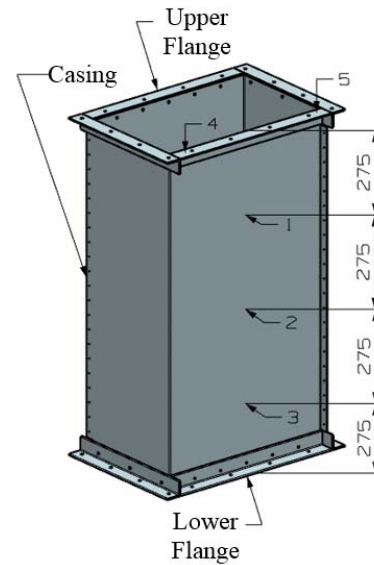Fig.13. Configuration of equipment and instrumentation for experimental test.

Fig.14. Position of the measuring instruments – unit.: *mm* .

Figure 14 shows the position of the measuring instruments on the sample. Points *1, 2* and *3* correspond to measurement of the lateral displacement of the plate and assist in the way of allocation of initial geometric imperfections in the model in the FEM. Points *4* and *5* are used to observe the moment of collapse of the box profile.

4.2. Experimental test results

To obtain the collapse load of the box profile a load cell signal reception system was positioned close to the dial indicator points *4* and *5* of Fig.14. This way, when the dial indicators showed an abrupt displacement towards the load, at one time it was viewed and taken as the box profile collapse load. Table 4 shows the values of collapse load of samples subjected to compression test centered, with the average and standard deviation.

Table 4. Experimental values of the box profile collapse.

Sample	Collapse Load (*kgf*)
1	*13100*
2	*13400*
3	*12900*
4	*13500*
Average	***13225***
Standard Deviation	*275*

Measurements performed at points *1, 2* and *3* were taken at every *1000 kgf* compressive load applied, shown in Tabs 5 to 8. The positive values of the measurements represent a plate displacement on the external side of its cross section, this way the negative values of the measurements represent a displacement in the internal side of its cross section. The result of the collapse load is also presented for each table. The asterisk (*) in the column of the load represents the measurements obtained after the collapse, and the double asterisk (**) represents the measure unassigned due to the use of the dial indicator at point *2*.

From the results and observations made during the experimental test, it was possible to create the deflection representation of the side plate of the box profile, shown in Figs 15 and 16 in a *5x* scale, for the samples 2 and 4.

Table 5. Results of measurements at points *1, 2* and *3* of sample 1.

Sample 1			
Load (*kgf*)	P.1 (*mm*)	P.2 (*mm*)	P.3 (*mm*)
1000	*0,000*	*0,12*	*0,000*
2000	*0,291*	*0,52*	*0,089*
3000	*0,872*	*1,25*	*0,339*
4000	*1,356*	*2,10*	*0,750*
5000	*1,791*	*3,00*	*1,107*
6000	*2,114*	*3,55*	*1,321*
7000	*2,857*	*4,32*	*1,660*
8000	*3,518*	*4,90*	*1,928*
9000	*4,584*	*5,50*	*2,284*
10000	*4,535*	*6,00*	*2,713*
11000	*4,939*	*6,30*	*2,677*
12000	*5,261*	*6,50*	*2,427*
13000	*5,471*	*6,58*	*2,106*
13100	**Collapse**		
*	*11,681*	**	*-17,259*

Table 6. Results of measurements at points *1, 2* and *3* of sample 2.

Sample 2			
Load (*kgf*)	P.1 (*mm*)	P.2 (*mm*)	P.3 (*mm*)
1000	*0,000*	*0,08*	*0,000*
2000	*0,048*	*0,43*	*0,268*
3000	*0,387*	*1,38*	*0,660*
4000	*0,662*	*1,80*	*1,142*
5000	*1,791*	*2,80*	*1,606*
6000	*3,083*	*3,78*	*1,945*
7000	*3,793*	*4,12*	*1,678*
8000	*4,261*	*4,28*	*0,928*
9000	*4,680*	*4,40*	*0,303*
10000	*5,229*	*4,50*	*-0,410*
11000	*7,343*	*4,70*	*-3,195*
12000	*8,538*	*4,85*	*-4,765*
13000	*9,684*	*4,92*	*-6,389*
13400	**Collapse**		
*	*12,444*	**	*-19,954*

The representation was created considering that the upper and lower ends of the side plate have no displacement and the measures at points *1, 2* and *3* regarding the loads of *7, 9, 11, 13* $(10^3 \ kgf)$ and after collapse were used. Each measurement taken on the side of the plate was represented by a dashed horizontal

line in the direction of numbers relating to the respective points. The dashed vertical line represents the undeformed plate. Considering that the plate is continuous, the end point of each dashed horizontal line and the ends were connected with a solid line, which is the approximate displacement of the side plate for each load previously described.

Table 7. Results of measurements at points *1, 2* and *3* of sample 3.

Sample 3			
Load (*kgf*)	**P.1 (*mm*)**	**P.2 (*mm*)**	**P.3 (*mm*)**
1000	*0,226*	*0,26*	*0,000*
2000	*1,081*	*1,01*	*0,161*
3000	*2,211*	*2,04*	*0,553*
4000	*3,454*	*3,28*	*0,821*
5000	*4,697*	*4,52*	*0,982*
6000	*5,778*	*5,62*	*1,196*
7000	*6,827*	*6,64*	*1,428*
8000	*7,795*	*7,62*	*1,785*
9000	*8,748*	*8,56*	*2,070*
10000	*9,603*	*9,44*	*2,320*
11000	*10,345*	*10,20*	*2,445*
12000	*10,943*	*10,70*	*2,481*
12900	**Collapse**		
*	*13,573*	**	*-16,427*

Table 8. Results of measurements at points *1, 2* and *3* of sample 4

Sample 4			
Load (*kgf*)	**P.1 (*mm*)**	**P.2 (*mm*)**	**P.3 (*mm*)**
1000	*0,178*	*0,27*	*0,000*
2000	*0,759*	*0,94*	*0,196*
3000	*1,533*	*1,91*	*0,750*
4000	*2,147*	*2,86*	*1,374*
5000	*2,954*	*4,01*	*2,124*
6000	*3,680*	*5,09*	*2,838*
7000	*4,132*	*5,84*	*3,105*
8000	*4,567*	*6,54*	*3,266*
9000	*4,955*	*6,98*	*3,302*
10000	*5,294*	*7,26*	*3,302*
11000	*5,842*	*7,46*	*2,641*
12000	*6,472*	*7,63*	*1,856*
13000	*7,343*	*7,78*	*0,910*
13500	**Collapse**		
*	*12,556*	**	*-14,653*

For the choice of buckling mode, which through its deformed geometry will represent and assign geometric imperfections in the numerical finite element model, it will be necessary to understand the evolution of the side of the box profile deflections. As the compression load is applied, the side of the box profile forms one deflection curve in the external direction of its cross section, an effect that was observed in Figs 15 and 16

from the load of *7000kgf* . However, when the box profile is very close to its collapse the side of the box profile forms two deflection curves, approximately half in the external direction and half in the internal direction of its cross section. In Fig.15 (sample 2) it is observed that this phenomenon is observed more clearly with *11000kgf* load when the side of the box profile began to show the change in the direction of deflections. Due to its final form (after collapse) you can see that in sample 4 (Fig.16) this phenomenon happened between *13000kgf* load and collapse.
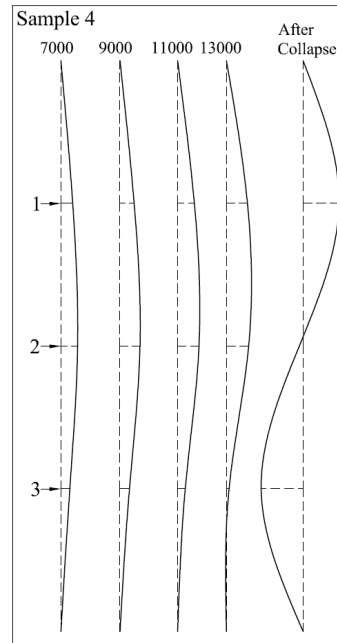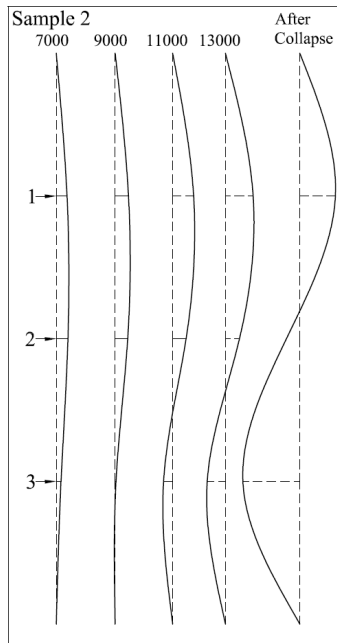

Fig.15. Deflection representation of the side plate of the box profile sample 2 (Scale: 5x) - unit: *kgf* .

Fig.16. Deflection representation of the side plate of the box profile of sample 4 (Scale: 5x) - unit: *kgf* .

It is worth emphasizing that, despite having not performed the measurements on both sides of the box profile, the same behavior was observed on both sides. Figure 17 shows the local effect due to the collapse of the box profile.
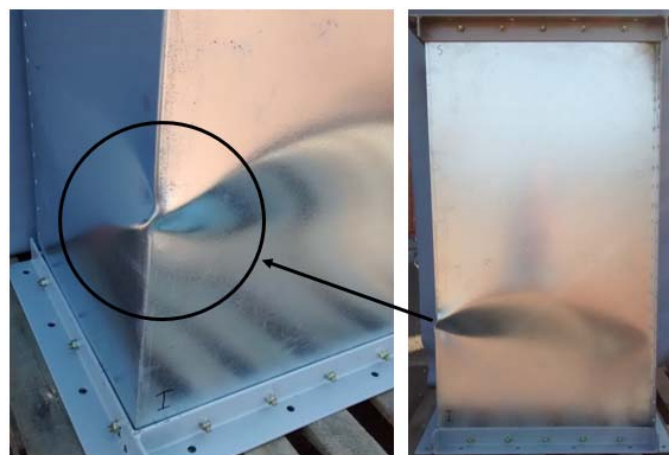

Fig.17. Local effect of the box profile collapse.

5. Structural analysis of box profile via finite element methods (FEM)

In what follows, we will describe the analysis procedures and the preparation of numerical models, how the assumptions and simplifications were made, obtaining the physical and geometrical properties, boundary conditions, loading and results.

5.1. Finite element methods (FEM): linear and nonlinear analysis

According to Alves Filho [24], the finite element method performs the analysis model in a finite number of parts called elements. These elements are connected to each other through connection points called nodes. This subdivision is called discretization of the system or discrete systems. From the understanding of the interaction behavior of each element it will be possible to understand the behavior of the entire structure.

With the assistance of computers, the main objective of finite element programs is to solve the main objective of final element programs is to numerous algebraic equations generated from the structural equilibrium conditions of each element that is discretized in the system. In the analysis of structural problems, the system solution is to find the displacements of the nodes, also called nodal displacements which are the unknowns of the problem.

As described by Bathe [25], in a linear analysis the responses of a system are linearly proportional to the loads applied in the same subject, and through the discretizing, the equation system (5.1) is obtained by means of the finite element:

$$[K_L][U] = [P]. \tag{5.1}$$

The matrix [P] contains the nodal forces applied to the system. The matrix $[U]$ is the one that provides the system responses through the nodal displacements that make it possible to obtain the stresses and strains of the system. The system stiffness matrix $[K_L]$ contains the proportionality factors of the strength with displacements and takes into account the physical properties of materials and the geometric properties. In the linear analysis, the stiffness matrix is a constant, meaning that it does not vary throughout the simulation.

In a nonlinear analysis, as pointed out by Bathe [25] the nodal strengths and displacements of the system have a non-linear behavior and, as opposed to a linear analysis, the stiffness matrix is not constant. In a nonlinear analysis, the equation system (5.2) is obtained by discretization using the finite element:

$$[K_{NL}(U)][U] = [P]. \tag{5.2}$$

The stiffness matrix $[K_{NL}(U)]$ for the nonlinear analysis is not constant and can be written as a function of displacements. In this case, it is not possible to obtain a direct displacement vector $[U]$. For their obtainment iterative methods are used, and among them the Newton-Raphson method can be mentioned. According to Chen *et al*. [26] it is generally used when the load versus displacement relation is monotonically increasing, in other words, when increasing the amount of the displacements there is no decrease in load values.

According to Alves Filho [20] in the nonlinear analysis the stiffness matrix of the structure consists of the basic stiffness matrix $[K]$ and geometric stiffness matrix $[K_G]$, and then $[K_{NL}(U)] = [K] + [K_G]$. The geometric stiffness matrix $[K_G]$ considers the interaction between the axial strength and displacements in the element and is considered a correction of the basic stiffness matrix. Therefore, with the rigidity of the beginning of each interval, known as the starting rigidity, and the correction proposed by the geometric stiffness matrix, it is possible to calculate the stiffness matrix of that iteration to the correct calculation of the displacements due to the load increase of the same iteration. Another important application of the geometric stiffness matrix,

engaging the effects of the axial strength on bending, is to evaluate the effects of elastic instability, where it is possible to calculate the value of the critical load that causes instability in the structure.

The nonlinearity of a system can have multiple origins, however, this article uses two types of non-linearity: non-linearity which corresponds to the properties of materials; and geometric nonlinearity, when large deflections change the equilibrium equations thus altering the stiffness of the structure as the load is applied.

To obtain the deformed geometry of the numerical model, which was used to assign the initial geometric imperfections, a linear instability analysis was performed using the eigenvalue and eigenvector method. To evaluate the load collapse, a nonlinear analysis was performed.

5.2. Physical constitutive relation of the material

The physical constitutive relation of the material relates the stresses with the strains. For numerical analysis in the FEM the material was considered to be homogeneous and isotropic. The linear instability analysis was performed using a linear elastic diagram. Non-linearity of the materials represented by multilinear diagram, was used for nonlinear analysis.

Maggi [27] uses in his work the bi-linear diagram, which consists of two straight segments that divide the elastic phase and plasticization of the material. The inclination in the elastic material phase is represented by the Young modulus (E) and the inclination in the plasticizing phase of the material is represented using the tangent modulus (E_t). Maggi [27] uses in his work the tangent modulus (E_t) being *10%* of the Young modulus (E).

Chodraui [11] uses in his work an approximation in a multilinear curve from characterization tests of the material used in his research. Yu [19] states that for a hot rolled steel plate the stress-strain curve is the sharp-yielding type, as shown in Fig.18, where F_y represents the yield stress of the material and F_u represents the ultimate tensile stress.
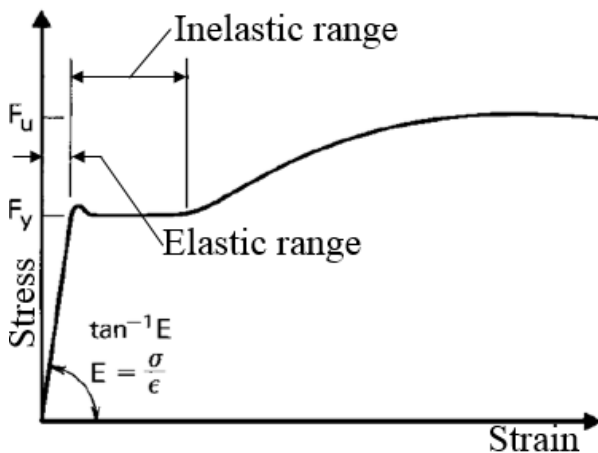

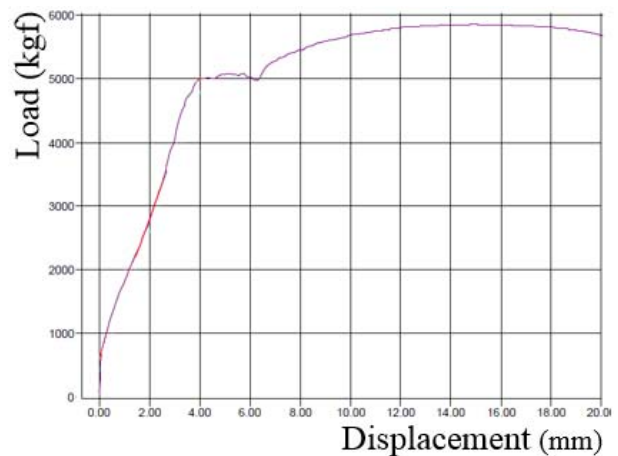Fig.18. Stress-strain curve for hot rolled steel plate.   Fig.19. Real graphic of the tension test.

This can be confirmed when compared to the real diagram of the tension test of a sample made from a hot rolled steel plate, as shown in Fig.19.

In this article, in following Chodraui [11], the stress-strain curve will be a multilinear approach to characterization tests of the used material, as shown in Fig.20, where, σ_y represents the material yield stress, σ_u represents the maximum ultimate tensile stress, ε_y is the strain of the material when it reaches the yield stress, ε_y' is strain at the end of inelastic phase and ε_u is strain when the material reaches its maximum ultimate tensile stress.
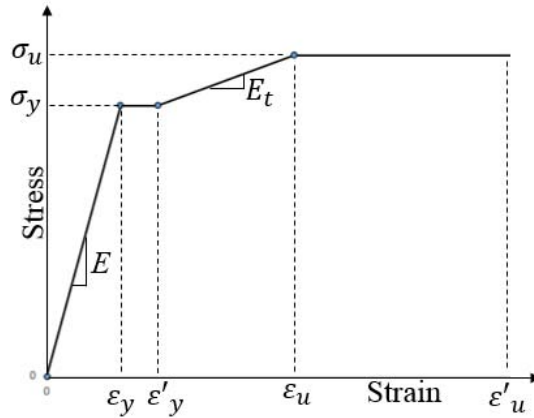
Fig.20. Multilinear approach of the stress-strain curve.

The value of Young's modulus (E) was assumed to be *200 GPa* and Poisson's coefficient of *0,3* according to standard ABNT NBR 14762 [1]. Taking into account the definitions of Maggi [27], the tangent modulus of the material (E_t) *10%* of the Young's modulus (E) was used.

At the time of cutting the sheets for subsequent manufacture of box profiles, a sample of the same sheet was taken for the tension test. Then, in total 4 samples were subjected to tension test to obtain the value of the yield strength and ultimate tensile stress of the material. Table 9 shows the results of tension test of the samples.

Table 9. Tension test result.

N.S.	Y.L. (*N*)	B.L. (*N*)	Y.S. (*MPa*)	U.T.S. (*MPa*)
1	5097,40	6030,22	269,70	319,06
2	5011,72	5862,72	265,17	310,20
3	4667,17	5507,60	246,94	291,41
4	4866,95	5876,12	257,51	310,91
A.	4910,81	5819,17	259,83	307,90
S.D.	188,22	221,18	9,96	11,70

Here, Y.L. is the yield load, B.L. is the breaking load, Y.S. is the yield stress, U.T.S. is the ultimate tensile stress, N.S. is the number of the samples, A. is the average and S.D. is the standard deviation.

Table 10. Pair of points of the multilinear stress-strain curve.

Stress (Mpa)	Strain
σ_y : 259,83	$\varepsilon_y = \dfrac{\sigma_y}{E}$: 0,00129915
σ_y : 259,83	$\varepsilon'_y = 1.5\varepsilon_y$: 0,00194872
σ_u : 307,90	$\varepsilon_u = \dfrac{(\sigma_u - \sigma_y)}{E_t} + \varepsilon'_y$: 0,00435222
σ_u : 307,90	$\varepsilon'_u = 2\varepsilon_u$: 0,00870445

Table 10 shows the values of the pair stress-strain for the creation of the material characterization curve. It is noteworthy that the strain values were obtained from the stress, Young's modulus and tangent modulus. The proportion of the strains $\varepsilon'_y e\ \varepsilon_y$, $\varepsilon'_u e\ \varepsilon_u$ were observed from the tension test of the samples.

5.3. Considerations and assignments of the initial geometric imperfections in numerical simulation

For validation of the boundary conditions of the numerical analysis a model with the same dimensions as the experimental model was used.

The geometric imperfections will be assigned only in the body of the box profile. Thus, a simplified model on surfaces was created without considering the flanges of the box profile and the point connection by sheet metal clinching.

For the finite element analysis of the box profile, the plates of the cold formed sections were represented by a plane surface of the medium modeled with shell elements. Figure 21 shows the boundary conditions assigned in the numerical model for linear buckling analyzes.
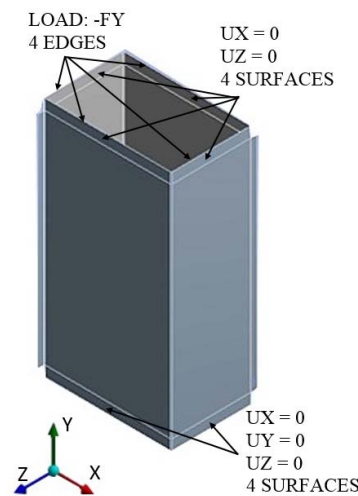

Fig.21. Assigned boundary conditions in the numerical model.

Elements of *8mm* were used for the numerical analyzes. They were chosen through a numerical evaluation of cost-benefit, where the cost is the time spent in processing of the calculation, and the benefit is the result with a *5 %* convergence.

As previously described, the side of the box profile evolves its configuration deflections, until the instant immediately before the collapse, to a form two curves. Thus, comparing the form of the deflections in the instant immediately before the collapse of the box profile in the experimental test with the deformed configuration shown in the cutting of the box profile section in Fig.4, it is possible to note that the first buckling mode is more similar between them, which also has two deflections curves on the side. Therefore, the assignment of geometric imperfections in the numerical model for the nonlinear analysis will be from the deformed configuration of the first mode of the linear elastic buckling.

5.4. Nonlinear finite element analysis of the numerical experimental model (EM)

Multiplication factors were analyzed with values of *0.20, 1, 2, 3, 4* and *5* to assess the influence on the collapse load.

Using the deformed geometry of the first buckling mode of the box profile body, the upper and lower flanges were modeled using shell elements. The flange material was modeled as being linear elastic and to represent the rigidity of the fixed devices on the flanges during experimental testing, its Young's modulus was

considered five times greater than the box profile material. The contacts between the flanges and the box profile, and the connection with sheet metal clinching were considered glued. Geometric non-linearity was considered in the analysis, in other words, the large strains and large rotation were considered. The application of the load was performed through steps with increases of *1000 N* each one. The analysis was initiated and allowed to elapse until the time of convergence loss.

Figure 22 shows the boundary conditions which were assigned in numerical model for the nonlinear analysis.
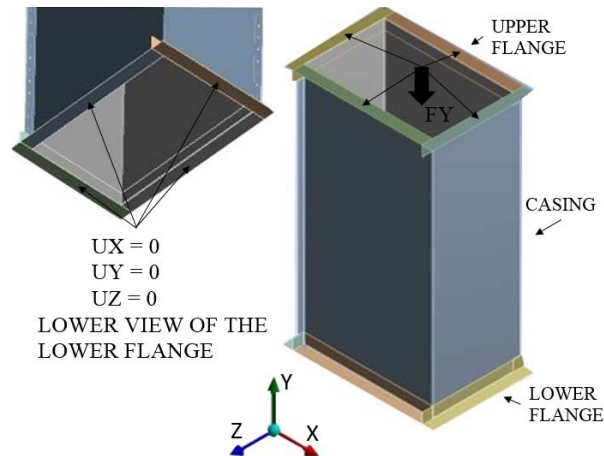

Fig.22. Model boundary conditions for nonlinear numerical analysis.

The values of the initial geometric imperfections (δ) were taken as the apex of the curve of the deflections first buckling mode, as shown in Fig.5, which was used to assign them.

Figure 23 shows the collapse load of the box profile and Fig.24 shows the greatest deflection found in the nonlinear analysis of MEF before the collapse, both depending on the multiplication factor and the initial geometric imperfection.
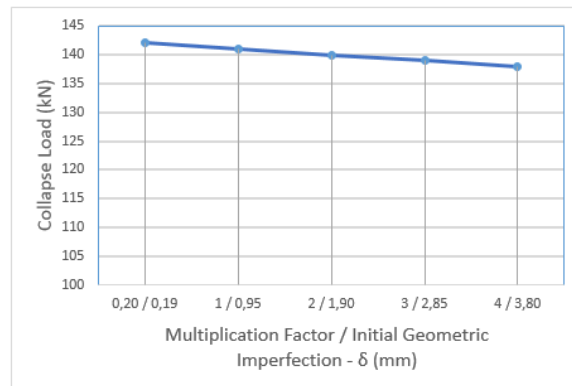

Fig.23. The adjective collapse load versus multiplication factor and geometric imperfection.

Analyzing Figs 23 and 24 it can be seen that the magnitude of the initial geometric imperfection has little influence on the results. The biggest difference in the values of the collapse load is only *4,3* %.

Unlike sections analyzed by Chodraui [11], the section formed by the box profile is closed and robust. This way, the box profile section, when submitted to compression stresses did not collapse under the critical buckling stress, but it presented a great post buckling resistance and collapsed by yielding due to the effect of local buckling.
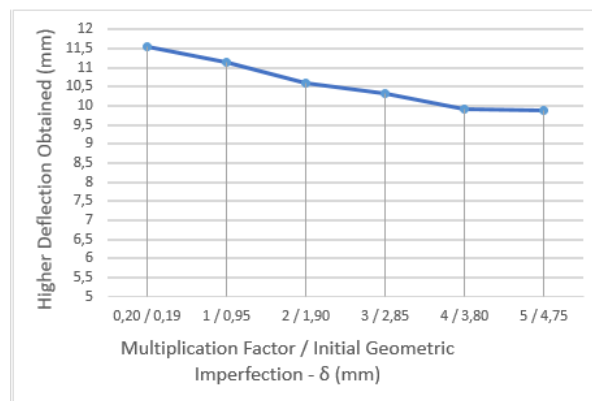
Fig.24. The greatest deflection obtained in numerical analysis versus multiplication factor and initial geometric imperfection.

The magnitude of the imperfections in the samples was not measured, but it should be considered that the machines involved in the box profile manufacturing process are precise. Thus, considering defects or initial imperfections with a large magnitude would not agree with the reality.

It was possible to observe in the nonlinear analysis in the FEM of the box profile under centered compression load that the initial geometric imperfections do not affect the result of the collapse load. Thus, the lateral of the box profile has little contribution to the section resistance, location where the initial geometric imperfections were assigned.

It is worth noting that the assignment of the initial geometric imperfections is very important in the analysis under compressive load. In addition, they serve as a guide for the deflections as the box profile reaches its collapse in the form of two curves, as previously described. If there were no imperfections in the box profile sections, it would simply lower its height and provide a constant strain throughout its side, which does not represent the reality.

Thus, it took up the multiplication factor of the deflection displacement to the value of *0,20*, where the maximum initial geometric imperfection is *0,19mm* . If the thickness of the experimental model box profile sheet is *1,55mm*, there is a relationship of *d/t* of *0,12*, close to *0,14* as reference statistical data of Schafer and Pekoz [12]. Therefore, the result of the collapse load of the box profile experimental model (EM) under centered load in the simulation by nonlinear finite element method was *144kN*.
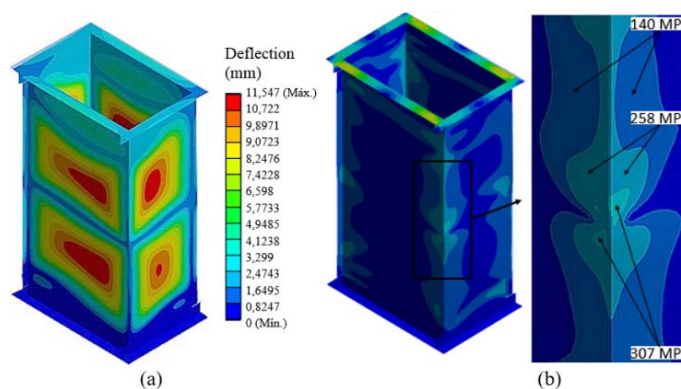

Fig.25. (a) Deflections on the EM box profile in the nonlinear numerical analysis; (b) Stresses on the EM box profile in the nonlinear numerical analysis.

Figure 25 (a) shows the deflections and Fig.25 (b) shows the stresses on the EM box profile in color scale related to the nonlinear FEM analysis with a load of *144kN*. It is possible to observe that the bends support the box profile section because they present a concentration of stresses.
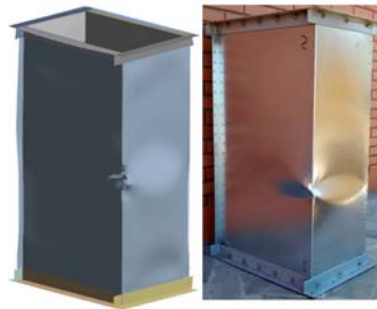

Fig.26. Comparison of numerical and real shape after collapse.

Figure 26 shows the similarity between the images of numerical analysis at the point of convergence loss, which is the collapse of the box profile with the actual image of the box profile section collapse in the experimental test.

5.5. Nonlinear finite element analysis on numerical model with original dimensions (MOD)

In the non-linear analysis by the finite element method of the box profile model with original dimensions (MOD) under compression load, the same boundary conditions applied to the experimental model presented in Figure 22. Just like in the experimental model, the deformed geometry of the first buckling mode was used as assignment of the initial geometric imperfections. Regarding the magnitude of imperfections a multiplication factor of the deflection of *0,4* was used, where its maximum initial geometric imperfection was *0,35*. When the thickness of the box profile sheet in the model with original dimensions is *2,70 mm*, a relation of d/t the value of *0,13* is obtained, close to *0,14* as reference statistical data of Schafer and Pekoz [12]. Therefore, the result of the model collapse load with original dimensions of the box profile was *393 kN*.
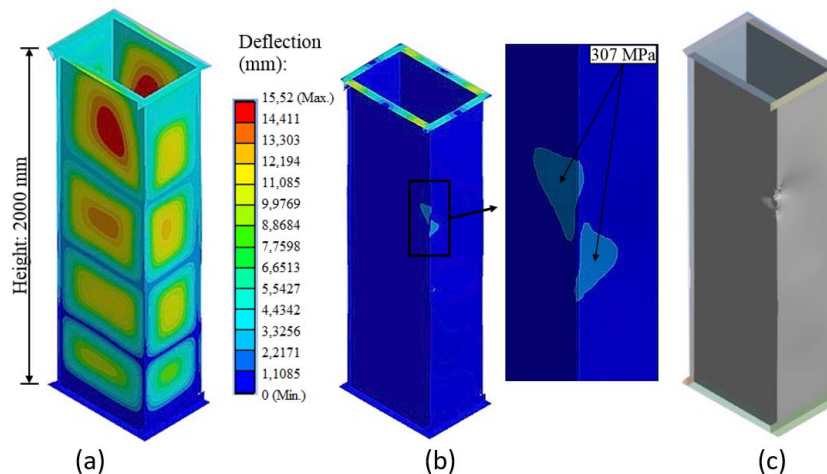

Fig.27. (a) Deflections on the MOD box profile in the nonlinear numerical analysis; (b) Stresses on the MOD box profile in the nonlinear numerical analysis; (c) Numerical Shape after collapse in MOD.

Figure 27(a) shows the deflections and Fig.27(b) shows the stresses on the MOD box profile in color scale related to the non-linear FEM analysis with a load of *393 kN*. Figure 27 (c) presents the region where there was a loss of convergence, representing the collapse of the box profile.

6. Conclusion

The experimental model of the box profile was evaluated by different methods. Initially, the value of the box profile collapse load was obtained by the effective width method, after that, by the experimental method. It was possible to obtain the approximate value of the collapse load and determine that the local buckling effect predominates at the time of the collapse.

In the test it was possible to see that the collapse of the box profile is really due to the effect of local buckling, as estimated in the calculations in the EWM. In addition, measurements were made on the side of the box profile deflection to understand the effect of compression load applied to the same and determine that the first buckling mode would be a better representation to assign geometric imperfections in the nonlinear analysis by the FEM.

In the non-linear analysis by the FEM, it was noted that although the magnitude of the geometric imperfections has little influence on the result of the box profile collapse load, it is a very important parameter to predict the loads of collapse due to the effects of buckling. The analysis methodology employed in this work showed that in the cross section of the box profile type, with cross section geometry formed by "flat panels" (flat side of the gutter) fixed in "curved panels" (the folds), the compression load action results in a redistribution of stresses, such that its strength is established mainly in the sheet bends that make up the box profile, a situation for which the eigenvalue method has difficulties in predicting the instability load, since the actual collapse load of the profile is greater than the load calculated by the method. Furthermore, initial imperfections serve as a guide to the deflection of the box profile sides so that the collapse of the non-linear FEM was the same as found in the experiment test. Table 11 presents the values of collapse load of the experimental model (EM) of the box profile type for the three methods used in the article. The average collapse load obtained in the experimental test (ET) was taken as a base. Compared with other analyzes, a load factor was obtained of 1,068 for the EWM and *1,110* for the FEM, representing a difference, respectively, *6,8*% and *11*%.

Table 11. Comparison of the results of the three evaluation methods in the EM box profile.

Analysis Method	Collapse Load (*N*)	Load Factor
ET	*129737*	*
EWM	*138570*	*1,068*
FEM	*144000*	*1,110*

For the model with the original dimensions (MOD) the analysis was performed by the EWM and FEM. Table 12 presents the analysis method (A.M.), the collapse load (C.L.), the load factor (L.F.), the collapse load multiplied by load factor (C.L.L.F.) and the percentage difference (P.D.).

Table 12. Comparison of the results of the two evaluation methods in the MOD box profile.

Analysis Method	Collapse Load (*N*)	L.F.	C.L.L.F. (*N*)	P.D. (%)
EWM	*380110*	*1,068*	*355908*	*0,52*
FEM	*393000*	*1,110*	*354054*	

Due to the cross section of the box profile type presenting geometric changes (flat elements joined to curved elements), and therefore the redistribution of stresses for the bends, the actual collapse load of the

profile is greater than the load calculated by the EWM method. Methodologies that better describe the local buckling behavior and verify the precepts of the existing norms on the subject, combining theoretical and experimental methods, contribute as they bring a better understanding of the problem in question. Thus, the presentation of this work used a methodology that describes the local buckling behavior and verified the precepts of the existing norms on the subject, combining theoretical and experimental methods, as they bring a better understanding of the problem in question. Therefore, an alternative for the analysis of instability of the box profile type is the methodology presented in this article, which also allows a better understanding of the structural problem under study.

Nomenclature

A.	– average
A_{ef}	– effective area of the cross section
b_a	– width of the element section
b_b	– width of the element section
B.L.	– breaking load
C_w	– torsional warping constant of cross section
E	– Young's modulus
E_t	– tangent modulus
f_u	– ultimate tensile stress
f_y	– yield stress
F_u	– ultimate tensile stress
F_y	– yield stress of the material
G	– shear modulus
I_x	– moment of inertia about the x-axis
I_y	– moment of inertia about the y-axis
J	– torsion constant of cross section
k	– plate-buckling coefficient of element
K	– effective length factor
$[K]$	– basic stiffness matrix
$[K_L]$	– stiffness matrix
$[K_{NL}(U)]$	– stiffness matrix
$[K_G]$	– geometric stiffness matrix
L	– height of the section
N_e	– the smallest value of the three-axial strength for overall buckling
$N_{c,\,Rd}$	– axial compressive strength
N.S.	– number of the samples
$[P]$	– matrix of the nodal forces
r_o	– polar radius of gyration of cross section about shear center
S.D.	– standard deviation
$[U]$	– matrix of nodal displacements
U.T.S.	– ultimate tensile stress
Y.L.	– yield load
Y.S.	– yield stress
ε_u	– strain when the material reaches its maximum ultimate tensile stress
ε_y	– strain of the material when it reaches the yield stress

ε'_y – strain at the end of inelastic phase

λ_o – overall buckling

λ_p – reduced slenderness factor of element

ν – Poisson's ratio

σ – critical stress

σ_u – maximum ultimate tensile stress

σ_y – material yield stress

χ – compression strength reduction factor

References

[1] ABNT - Brazilian Association of Technical Standards (2010): *NBR 14762: Design of steel structures made of cold-formed profiles*.– In Portuguese.

[2] Chou S. M., Chai G. B. and Ling L. (2000): *Finite element technique for design of stub columns*.– Thin-Walled Struct., vol.37, pp.97-112.

[3] Narayanan S. and Mahendran M. (2003): *Ultimate capacity of innovative cold formed steel columns*.– Journal of Constructional Steel Research, vol.59, pp.489-508.

[4] Lecce M. and Rasmussen K.J.R. (2005): *Finite element modelling and design of cold-formed stainless steel sections*.– Sydney, Australia. Department of Civil Engineering, University of Sydney, Research Report R845.

[5] Chryssanthopoulos M.K., Baker M.J. and Dowling P.J. (1991): *Imperfection modeling for buckling analysis of stiffened cylinders*.– Journal of Structural Engineering, vo.177, No.7.

[6] Triches F.J. (2011): *Structural analysis of the support columns of a metallic silo* (in Portuguese).– School of Engineering, Federal University of Rio Grande do Sul, Porto Alegre.

[7] Almeida, S.J.C. (2007): *Numerical analysis of compressed cold formed steel profiles considering initial geometric imperfections* (in Portuguese).– São Carlos School of Engineering, University of São Paulo, São Carlos.

[8] Galambos, T.V. (1998): *Guide to Stability Design Criteria for Metal Structures*.– New York: John Wiley & Sons, p.911.

[9] Batista E.M. and Rodrigues F.C. (1994): *Buckling curve for cold-formed compressed members*.– Journal of Constructional Steel Research, vol.28, pp.121-136.

[10] Rasmussen K.J.R. and Young B. (1998): *Tests of fixed-ended plain channel columns*.– Journal of Structural Engineering, ASCE, vol.124, No.2, pp.131-139.

[11] Chodraui G. M. B. (2006): *Theoretical and experimental analysis of cold formed steel profiles subjected to compression* (in Portuguese).– PhD Thesis, São Carlos School of Engineering, University of São Paulo, São Carlos.

[12] Schafer B. W. and Peköz T. (1998): *Computational modeling of cold-formed steel: characterizing geometric imperfections and residual stresses*.– Journal of Constructional Steel Research, vol.47, pp.193-210.

[13] Limam A.; El Bahaoui J., Khamlichi A. and El Bakkali L. (2011): *Effect of multiple localized geometric imperfections on estability of thin axisymmetric cylindrical shells under axial compression*.– International Journal of Solids and Structures, vol.48, pp.1034-1043.

[14] Chen Y., Ganping S., Baofeng Z. and Ruihua L. (2019): *Local buckling behavior of welded π-shaped compression stub columns*.– Journal of Constructional Steel Research, vol.154, pp.224-234.

[15] Couto C. and Vila Real P. (2019): *Numerical investigation on the influence of imperfections in the local buckling of thin-walled I-shaped sections*.– Thin-Walled Structures, vol.135, pp.89-108.

[16] Bonatto R. (2009): *Study of structural behavior and optimization of cold formed steel angles* (in Portuguese).– School of Engineering, Federal University of Rio Grande do Sul, Porto Alegre.

[17] Young B. (2013): *Tests and Design of Fixed-Ended Cold-Formed Steel Plain Angle Columns*.– Journal of Structural Engineering, vol.130, No.12, pp.1931-1940.

[18] Souza F.T. (2013): *Theoretical-experimental analysis of the stability of perforated columns in cold formed steel profiles of rack-type sections* (in Portuguese).– PhD Thesis, School of Mines, University of Ouro Preto, Ouro Preto.

[19] Yu W.W. (2000): *Cold-Formed Steel Design*.– 3rd ed. New York: John Wiley & Sons, INC. p.515.

[20] Alves Filho A. (2012): *Finite Elements. The basis of CAE technology: Nonlinear Analysis* (in Portuguese).– São Paulo: Érica.

[21] Von Karman T., Sechler E.E., Donnell L.H. (1932): *The Strength of Thin Plates in Compression*.– Transactions ASME, vol. 54, pp.54-5.

[22] Carvalho P.R.M., de Grigoletti G. and Barbosa G.D. (2014): *Basic Course of Cold Formed Steel Profiles* (in Portuguese).– 3rd ed., Porto Alegre.

[23] ABNT - Brazilian Association of Technical Standards (2010): *NBR 8800: Design of steel structures and mixed steel and concrete structures of buildings*.– In Portuguese.

[24] Alves Filho A. (2007): *Finite Elements. The basis of CAE technology*.– 5th ed. São Paulo: Érica.

[25] Bathe K.J. (1996): *Finite Element Procedures*.– New Jersey: Prentice-Hall.

[26] Chen W. F. and Han D. J. (1988): *Plasticity for Structural Engineers*. New York: Springer – Verlag.

[27] Maggi Y. I (2000): *Numerical Analysis, via M.E.F., of the Behavior of Bolted Beam-Column Connections with Top Plate* (in Portuguese).– São Carlos School of Engineering, University of São Paulo, São Carlos.